Review for the Astronomische Gesellschaft to appear in Astronomische Nachrichten

Radio studies of galaxy formation: Dense Gas History of the Universe

C.L. Carilli[1], F. Walter[2], D. Riechers[3], R. Wang[1], E. Daddi[4], J. Wagg[5], F. Bertoldi[6], K. Menten[7]

ABSTRACT

Deep optical and near-IR surveys have traced the star formation history of the Universe as a function of environment, stellar mass, and galaxy activity (AGN and star formation), back to cosmic reionization and the first galaxies ($z \sim 6$ to 8). While progress has been truly impressive, optical and near-IR studies of primeval galaxies are fundamentally limited in two ways: (i) obscuration by dust can be substantial for rest-frame UV emission, and (ii) near-IR studies reveal only the stars and ionized gas, thereby missing the evolution of the cool gas in galaxies, the fuel for star formation. Line and continuum studies at centimeter through submillimeter wavelengths address both these issues, by probing deep into the earliest, most active and dust obscured phases of galaxy formation, and by revealing the molecular and cool atomic gas. We summarize the techniques of radio astronomy to perform these studies, then review the progress on radio studies of galaxy formation. The dominant work over the last decade has focused on massive, luminous starburst galaxies (submm galaxies and AGN host galaxies). The far infrared luminosities are $\sim 10^{13}$ $L_\odot$, implying star formation rates, SFR $\geq 10^3$ $M_\odot$ year^{-1}. Molecular gas reservoirs are found with masses: $M(H_2) > 10^{10}(\alpha/0.8)$ $M_\odot$. The CO excitation in these luminous systems is much higher than in low redshift spiral galaxies. Imaging of the gas distribution and dynamics suggests strongly interacting and merging galaxies, indicating gravitationally induced, short duration ($\leq 10^7$ year) starbursts. These systems correspond to a major star formation episode in massive

---

⋆The Very Large Array of the National Radio Astronomy Observatory, is a facility of the National Science Foundation operated under cooperative agreement by Associated Universities, Inc

[1]National Radio Astronomy Observatory, P.O. Box 0, Socorro, NM, USA 87801-0387

[2]Max-Planck Institute for Astronomy, Konigstuhl 17, 69117, Heidelberg, Germany

[3]Department of Astronomy, California Institute of Technology, MC 249-17, 1200 East California Boulevard, Pasadena, CA 91125, USA; Hubble Fellow

[4]Laboratoire AIM, CEA/DSM - CNRS - University Paris Diderot, DAPNIA/Service Astrophysccique, CEA Saclay, Orme des Merisiers, 91191 Gif-sur-Yvette, France

[5]European Southern Observatory, Casilla 19001, Santiago, Chile

[6]Argelander Institute for Astronomy, University of Bonn, Auf dem Hügel 71, 53121 Bonn, Germany

[7]Max-Planck Institute for Radio Astronomy, Auf dem Hugel 69,53121, Bonn, Germany

galaxies in proto-clusters at intermediate to high redshift. Recently, radio observations have probed the more typical star forming galaxy population (SFR $\sim 10^2$ $M_\odot$ year^{-1}), during the peak epoch of Universal star formation ($z \sim 1.5$ to 2.5). These observations reveal massive gas reservoirs without hyper-starbursts, and show that active star formation occurs over a wide range in galaxy stellar mass. The conditions in this gas are comparable to those found in the Milky Way disk. A key result is that the peak epoch of star formation in the Universe also corresponds to an epoch when the baryon content of star forming galaxies was dominated by molecular gas, not stars. We consider the possibility of tracing out the dense gas history of the Universe, and perform initial, admittedly gross, calculations. We conclude with a description and status report of the Atacama Large Millimeter Array, and the Expanded Very Large Array. These telescopes represent an order of magnitude, or more, improvement over existing observational capabilities from 1 GHz to 1 THz, promising to revolutionize our understanding of galaxy formation.

Subject headings: Galaxy formation, radio techniques, molecular gas, dust

1. Introduction

1.1. The optical view of galaxy formation

A dramatic advance in the study of galaxy formation over the last decade has been the delineation of the cosmic star formation rate density (the 'star formation history of the Universe'; SFHU) to a look-back time within 0.6 Gyr of the Big Bang (Madau et al. 1996; Bouwens et al. 2010). Three main epochs have been identified (Figure 1): the first is a gradual rise during cosmic reionization at $z \sim 10$ to 6, corresponding to the epoch when light from the first galaxies and quasars reionize the neutral IGM that pervaded the Universe (Fan et al. 2006). Second is the 'epoch of galaxy assembly' at $z \sim 1$ to 3, when the cosmic star formation rate density peaks, and during which about half the stars in the present day Universe form (Marchesini et al. 2009). And third is the order of magnitude decline in the comoving cosmic star formation rate density from $z \sim 1$ to the present, constituting the inexorable demise of galaxy formation with cosmic time, as we run out of cold gas.

These studies have progressed to the next level of detail, namely the SFHU as a function of galaxy environment, stellar mass, and star formation rate (SFR). One interesting result is the observation of 'downsizing' in galaxy formation. This entails the systematic decrease in specific star formation rate (SSFR; star formation rate per unit stellar mass), with increasing stellar mass (Cowie et al. 1997). Downsizing is a manifestation of the general fact that massive galaxies form most of their stars early and quickly, and the more massive, the earlier and quicker. Evidence includes studies of the evolution of the SSFR (Moresco et al. 2010), stellar population synthesis studies of nearby ellipticals (Renzini 2006; Collins et al. 2009), and the direct observation of evolved, passive

galaxies at high z (Kurk et al. 2009; Doherty et al. 2009; Andreon & Huertas-Company 2011).

A second interesting result is the shift of the balance of star formation to more actively star forming galaxies with increasing redshift. At $z \sim 0$, the cosmic star formation rate density is dominated by galaxies with star formation rates ≤ 10 $M_\odot$ year^{-1} (FIR luminosities $\leq 10^{11}$ $L_\odot$). By $z \sim 2$, the dominant contribution shifts to galaxies forming stars at ≥ 100 $M_\odot$ year^{-1} (Murphy et al. 2011; Magnelli et al. 2011).

1.2. The role of radio observations

The results above are based, for the most part, on observations at optical through near-IR wavelengths. While truly remarkable in scope, optical through near-IR studies of galaxy formation are limited in two fundamental ways. First, dust obscuration plays a substantial role in determining views of early galaxies, in particular, the most active star forming galaxies. The average correction factor for Lyman Break galaxies (LBGs) when deriving total star formation rates from UV luminosity entails a factor five increase from observed to intrinsic star formation rates. This technique has been refined through the use of UV spectral slopes (Calzetti et al. 1994; Daddi et al. 2004).

And second, optical/near-IR studies reveal the stars, but miss the cold molecular gas, the fuel for star formation in galaxies. There is a well established correlation between the Far-IR and CO luminosity of galaxies (Figure 2). This correlation is not surprising, given that stars form in molecular clouds (Bigiel et al. 2011), and it argues that the rapid evolution of star formation with redshift should be reflected in the evolution of the molecular gas content of galaxies.

Observations at centimeter through submm wavelengths solve both these issues. Radio observations probe deep into the earliest, dusty, most active phases of star formation in galaxies. Similarly, cm through submm observations reveal the cool molecular and atomic gas in galaxies.

Figure 3 shows an example of these phenomena in a luminous starburst galaxy at $z \sim 4$. The contours show the thermal emission from warm dust and the CO emission, while the greyscale is the HST i-band image. The dust and gas trace the regions of most active star formation, and these regions are completely obscured in the HST image.

2. Tools of radio astronomy

We briefly review some of the observational tools available to study the gas, dust, and star formation in distant galaxies.

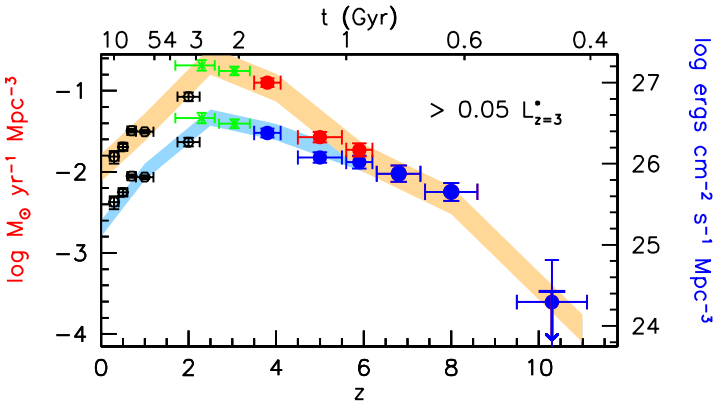

Fig. 1.— The evolution of the comoving cosmic star formation rate density as a function of redshift. The blue curve indicates star formation rates estimated from rest-frame UV measurements with no dust correction. The yellow curve includes the subtantial dust correction (from Bouwens et al. 2010).

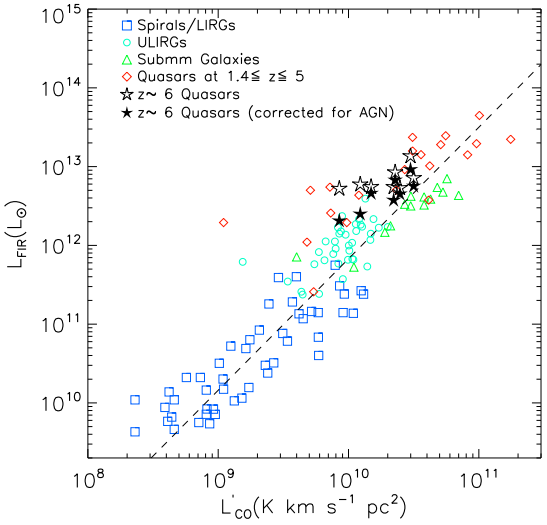

Fig. 2.— The correlation between Far-IR luminosity (L_{FIR}) and CO line luminosity (L'_{CO1-0}) for both low and high redshift star forming galaxies (from Wang et al. 2010).

2.1. Continuum

Figure 4 shows the SED at cm through FIR wavelengths of an active star forming galaxy redshifted to $z = 5$. The cm emission is synchrotron radiation from cosmic ray electrons spiraling in interstellar magnetic fields. These electrons are accelerated in supernova remnant shocks, and hence the radio luminosity will be proportional to the massive star formation rate. The FIR emission is from dust heated by the interstellar radiation field, which in active star forming galaxies is dominated by massive stars.

Hence, both the FIR and radio emission are a function of the massive star formation rate, resulting in the well quantified correlation between the radio and FIR luminosity from galaxies (Yun et al. 2001). While the tightness and linearity of the relationship over such a large range in luminosity remains puzzling, this correlation is an important tool for studying dust obscured star formation in galaxies, providing two means for estimating massive star formation rates in distant galaxies. Studies of galaxies at least out to $z \sim 2$ show that the correlation remains unchanged (Bourne et al. 2011), although at the highest redshifts it may be inevitable that inverse Compton scattering losses off the CMB by the relativistic electrons leads to a departure from the low z relationship (Carilli et al. 2008).

An important point is that FIR emission peaks around 100μm. For high redshift galaxies, this emission shifts into the submm bands. A related point is the well studied 'inverse-K' correction in the submm: the rapid rise in luminosity density on the Rayleigh-Jeans side of the modified grey body emission curve offsets distance losses, leading to a roughly constant observed flux density with redshift for a fixed observing frequency and intrinsic luminosity (Blain et al 2002). In essence, submm observations provide a distance independent method with which to study star forming galaxies.

For reference, for a typical dust temperature of $\sim$ 45K, the relationships between observed 350 GHz flux density (S_{350GHz}, in mJy), dust mass, integrated far-IR luminosity, and total star formation rate (SFR; Chabrier IMF) are approximately:

$$L_{IR} = 1.5 \times 10^{12} S_{350\mathrm{GHz}}\ \mathrm{L}_\odot$$

$$M_{dust} = 7.6 \times 10^{-5}\ L_{IR}\ \mathrm{M}_\odot$$

$$\mathrm{SFR} = 1.0 \times 10^{-10} L_{IR}\ \mathrm{M}_\odot\ \mathrm{year}^{-1}$$

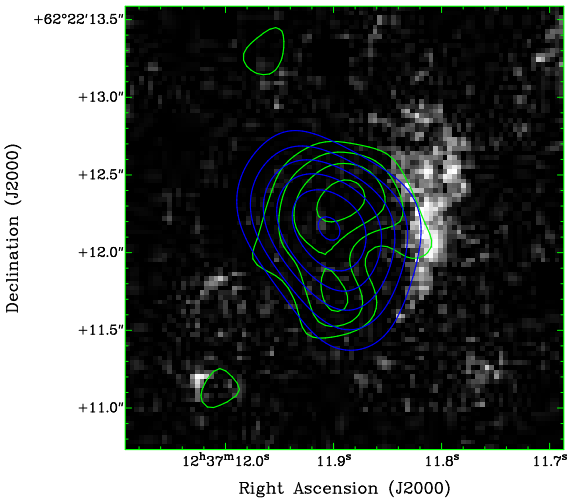

Fig. 3.— Blue contours show the 250GHz continuum emission from the $z = 4.0$ SMG GN20. Green contours show the CO 2-1 emissio. The greyscale shows the HST i-band image (from Carilli et al. 2010).

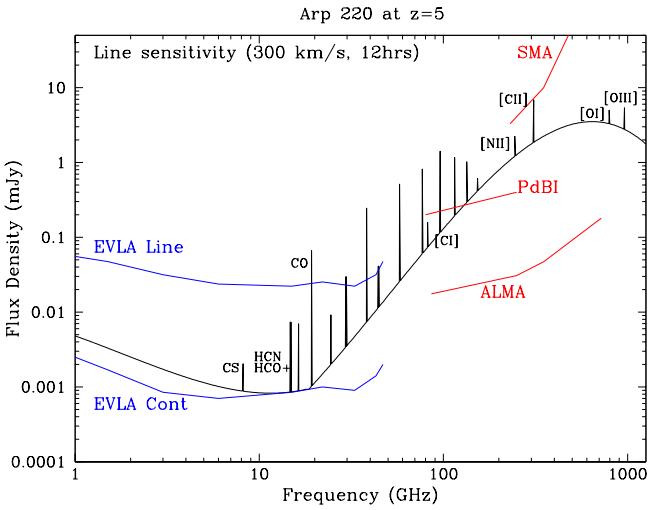

Fig. 4.— Radio through submm spectrum of a star forming galaxy with a star formation rate 100 $M_\odot$ year redshifted to $z = 5$. Also shown are the line and continuum sensitivity for the EVLA in 12 hours, and the line sensitivity for ALMA and the existing (sub)mm interferometers.

2.2. Molecular rotational transitions

A rich spectrum of rotational transitions of common molecules redshifts into the cm and mm bands for distant galaxies (Figure 4). Most prominent are the emission lines from CO. CO has long been used as a tracer for the total molecular gas mass (dominated by H_2):

$$M(H_2) = \alpha L'_{CO1-0} \quad M_\odot$$

where α is the CO luminosity to H_2 mass conversion factor. The units for L'_{CO1-0} are K km s^{-1} pc^2. These units were originally designed for spatially resolving observations of CO in the Galaxy, where brightness temperature was paramount.

Values of the CO luminosity to H_2 mass conversion factor α, range from 0.8 $M_\odot$/[K km s^{-1} pc^2] for luminous starburst nuclei in nearby galaxies, to 3.6 $M_\odot$/[K km s^{-1} pc^2] for Milky Way-type spiral disks. Since the CO emission is optically thick on small scales (ie. molecular cloud cores), α is calibrated essentially based on dynamical measures of masses, from virialized GMCs to gas dominated rotating disks in starburst nuclei (Downes & Solomon 1998). There is evidence for both values in the different populations of high z galaxies, again separated according to compact starbursts and star forming disk galaxies (Daddi et al 2010b; Tacconi et al. 2010; Genzel et al. 2010; Naraynan et al. 2011).

Solomon & vanden Bout (2005) derive the following relationships between CO luminosity and observed flux density and line width:

$$L'_{CO} = 3.3 \times 10^{13} S\Delta V D_L^2 \nu_o^{-2} (1+z)^{-3} \quad \text{K km s}^{-1} \text{ pc}^2$$

where ν_o is the observing frequency in GHz, the luminosity distance, D_L, is in Gpc, the flux density, S, is in Jy, and velocity width, ΔV, is in km s^{-1}. For CO luminosity in solar units the relationship is:

$$L_{CO} = 1.0 \times 10^3 S\Delta V (1+z)^{-1} \nu_r D_L^2 \quad L_\odot$$

where ν_r is the rest frequency in GHz. Solving for $S\Delta V$ in (4) and (5), and equating (Carilli 2011), yields:

$$L_{CO} = 3 \times 10^{-11} \nu_r^3 L'_{CO} \quad L_\odot$$

Other critical contributions of molecular line observations include:

- Gas velocities determine the dynamical masses of high$z$ galaxies, and internal gas dynamics in star forming regions.

- Multi-transition studies provide the gas excitation, which gives a rough estimate of gas density and/or temperature.
- Observations of high dipole moment molecules, such as HCN and HCO+, provide an estimate of the dense gas content of galaxies ($n(H_2) > 10^4$ cm^{-3}).

2.3. Atomic fine structure transitions

The atomic fine structure lines are emitted predominantly in the rest frame FIR, and hence redshift into the submm range for distant galaxies (Figure 4). Being metastable transitions, and hence typically optically thin, these lines, and in particular the [CII] 158μm line, are the principle coolant of interstellar gas (Spitzer 1998). The [CII] can carry up to 1% of the total IR luminosity from galaxies, and is typically the brightest line from IR through meter wavelenths (Malhotra et al. 2001; Bennett et al. 1994). The [CII] line traces the CNM and photon-dominated regions associated with star formation (Cormier et al. 2010). Fine structure line ratios can be used as an AGN versus star formation diagnostic (Genzel & Cesarsky 2000).

Herschel is providing a revolutionary view of these lines in nearby galaxies (Cormier et al. 2010). Submm telescopes are beginning to make serious in-roads into the study of these lines in distant galaxies (Stacey et al. 2010).

3. Molecular gas at high redshift

Figure 5 shows a histogram of the number of detections of CO emission from high redshift galaxies versus year. To date, there are 115 detections of CO at $z > 1$. The number of detections has almost doubled in the last two years due to two factors. First is improved instrumentation, in particular continued improvements at the Plateau de Bure Interferometer (PdBI), and the coming on-line of the EVLA and the GBT Zpectrometer.

More important is the change in the type of galaxies that are being discovered in CO emission in that last two years. Prior to 2009, the only galaxies that were detected in CO emission at high z were extreme starburst galaxies selected in wide field submm surveys (the submm galaxies, or SMGs), as well as the host galaxies of some very luminous quasars and radio galaxies. The only exceptions were a few highly gravitationally magnified Lyman Break Galaxies (LBG; Baker et al. 2004; Riechers et al. 2010b; Coppin et al. 2007). However, in the last two years a new class of galaxy has been detected in CO emission: more typical star forming disk galaxies at $z \sim 1$ to 3 selected via standard color-color techniques in optical and near-IR deep fields. These are a hundred times more numerous than the SMGs, and yet are often as luminous in CO emission.

4. Extreme starbursts: massive galaxy formation in the early Universe

4.1. General properties

Molecular gas detections of high redshift galaxies have focused primarily on extreme starburst galaxies at $z > 1$. These include highly dust obscured galaxies identified in wide field submm surveys (SMGs), as well as the host galaxies of optically selected luminous quasars, and some radio galaxies (Miley & de Breuck 2008). Typical submm surveys at 350 GHz detect galaxies at the few mJy level, implying $L_{FIR} \geq 10^{13}$ $L_\odot$ (ie. 'Hyperluminous infrared galaxies', HyLIRGs), dust masses $\sim 10^9$ $M_\odot$, and star formation rates $\geq 10^3$ $M_\odot$ year^{-1}. In parallel, about 1/3 of optically selected quasars from eg. SDSS, are detected with similar FIR luminosities. Solomon & Vanden Bout (2005) and Blain et al. (2002) present extensive reviews of these 'Extragalactic Molecular Galaxies,' and we update some of the information herein.

The areal density of SMGs at $S_{250} \geq 3$mJy is about 0.05 sources arcmin^{-2} (Bertoldi et al. 2010; Blain et al. 2002). The redshift distribution has been determined for about 50% of the SMGs selected using 1.4GHz continuum observations to determine arcsecond positions. The median redshift is $z \sim 2.3$, with most of the radio detected sub-sample within $z \sim 1$ to 3 (Chapman et al. 2003). However, recently it has become clear that there is a tail of SMGs extending to high redshift, with possibly 20% of the sources extending to $z \sim 5$ (Riechers et al. 2010a; Daddi et al. 2009a; 2009b; Schinnerer et al. 2008; Coppin et al. 2009).

The mean space density of the SMGs is $\sim 10^{-5}$ Mpc^{-3} at ~ 2. (comoving; Blain et al. 2002; Chapman et al. 2003). This space density is about 1000 times larger than for galaxies of similar FIR luminosity at $z = 0$, demonstrating the dramatic evolution in the number density of FIR luminous galaxies with redshift. Daddi et al. (2009a) conclude, based on SMG space densities and duty cycles, that there are likely enough SMGs at $z > 3.5$ to account for the known populations of old massive galaxies at $z \sim 2$ to 3. Study of the clustering properties of SMGs suggests a minimum halo mass of 3×10^{11} $M_\odot$ (Amblard et al. 2011). However, this calculation is somewhat problematic due to the low space density, the broad redshift selection function, and the likely low duty cycle of SMGs (Chapman et al. 2009).

Michalowski et al. (2010) present a detailed study of of the radio through UV SED of SMGs. They find a median stellar mass of 3.7×10^{11} $M_\odot$. The sources follow the radio-FIR correlation for star forming galaxies, except perhaps at the highest luminosities, where a low luminosity radio AGN may contribute. The dust temperatures span a broad range (10 K to 100 K), with a typical value $\sim$ 40K. They calculate that SMGs contribute about 20% of the cosmic star formation rate density at $z \sim 2$ to 4.

4.2. Molecular gas

Extensive observations have been performed of the molecular gas in SMGs and high redshift AGN host galaxies. Typical gas masses derived from observations of low order CO transitions range from 10^{10} $M_\odot$ to $10^{11} \times (\alpha/0.8)$ $M_\odot$ (Hainline et al. 2006;; Ivison et al. 2011; Riechers et al. 2010a, 2011c; Carilli et al. 2010; Wang et al. 2010).

Figure 6 shows the spectral energy distribution of the CO emission lines from a number of sources (Weiss et al. 2007). The excitation is uniformly high, significantly higher than is seen for the CO in the inner disk of the Milky Way. The excitation is comparable to what is found in the nuclear starburst regions on 100pc scales in M82 and NGC 253. Radiative transfer model fitting to the mean excitation indicates warm ($\geq$ 50 K), dense ($\geq 10^4$ cm^{-3}) molecular gas dominates the integrated CO emission from these galaxies. Such conditions are only found in the star forming cores of Giant Molecular Clouds in the Milky Way on parsec scales. The SMGs show systematically lower excitation than the QSO host galaxies, and there is mounting evidence for a lower excitation, more spatially extended molecular gas distribution in SMGs (Ivison et al. 2011, Harris et al. 2010; Riechers et al. 2010a; 2011c, Carilli et al. 2010, Papadopoulos et al. 2002; Scott et al. 2011).

High resolution CO imaging has been performed on a number of SMGs and AGN host galaxies. Figure 7 shows an example of the CO intensity and velocity field for the $z = 4.4$ quasar host galaxy, BRI1335-0417 (Riechers et al. 2008). In most cases, the CO emission appears to be complex, with two or more compact knots of emission separated by a few kpc (Tacconi et al. 2008; Carilli et al. 2002; Riechers 2008; 2011c). The velocity fields often appear chaotic, with little indication of rotation, however, this may not be universal for the low order emission (Carilli et al. 2011).

Figure 2 shows the integrated star formation law for both low redshift, lower luminosity star forming galaxies, and low and high redshift HyLIRG. There is a non-linear correlation between these two quantities over a broad range in luminosity. The relation is consistent with a powerlaw of index 1.5 between L'_{CO} and L_{FIR}. These two quantities are linearly related to total molecular gas mass and star formation rate (Section 2.1). Extensive analysis has gone into understanding this relationship physically, both for the integrated correlation, and the spatially resolved correlation in galaxies (Leroy et al. 2008; Bigiel et al. 2011; Kennicutt 1998; Krumholz et al. 2009; Narayanan et al. 2011). Regardless of the physical interpretation and α, the empirical implication of Figure 2 is that the FIR luminosity increases super-linearly relative to the CO luminosity of galaxies. A review of the physics of the star formation law is well beyond the scope of this review. Herein, we make a few simple, empirical points (see also Section 5.4).

First is that even the AGN sources follow this relationship, which is circumstantial evidence for star formation in the host galaxies as the dominant heating source for the warm dust (see section 4.3). And second is that the non-linearity of the relationship implies shorter gas consumption timescales ($\equiv$ M_{gas}/SFR) with increasing luminosities. For spiral galaxies like the Milky Way, with $L_{FIR} \sim 10^{10}$ $L_\odot$, the gas consumption timescale is a few $\times 10^8$ years, while for HyLIRGs this decreases to $\leq 10^7$ years, although this depends strongly on the assumed value of α (see section

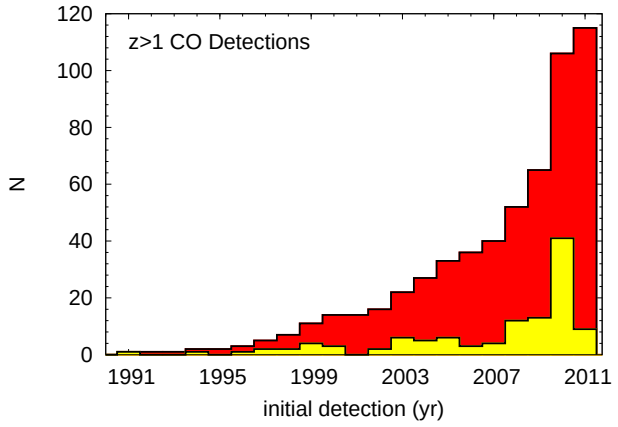

Fig. 5.— The number of new CO detected galaxies at $z > 1$ per years (yellow). Red is the cummulative curve.

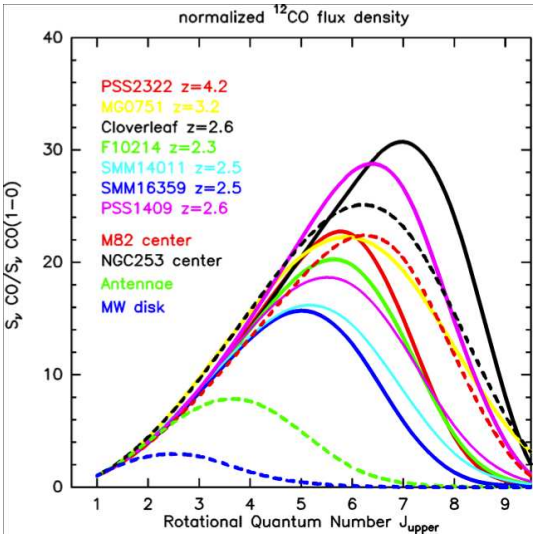

Fig. 6.— The CO excitation ladder for the integrated emission from high z SMGs and AGN hosts, plus the dashed lines show the inner disk of the Milky Way and selected nearby galaxies (from Weiss et al. 2007). The X-axis is the upper rotational level of the CO transition, while the Y-axis is the normalized flux from the CO line.

5.3).

Progress has also been made on detecting the dense gas tracers, such as HCO+ and HCN, from high redshift galaxies. These molecules are much less abundant than CO, but have much higher dipole moments, and hence stronger rotational transitions. This implies that the radiative lifetimes are much shorter, and hence maintenance of a Boltzmann distribution via collisions requires high densities, n(H_2) $> 10^4$ cm^{-3}, even for the lower states, and considerably higher for the higher order states. Hence, the high order states can be significantly sub-thermally populated, and emission from these molecules only comes from the densest molecular gas in galaxies. Interestingly, L_{FIR} and L'_{HCN} form a linear correlation (as opposed to the non-linear correlation with L'_{CO}; Gao & Solomon 2004). The simplest interpretation is that observations of these high density tracers simply 'count' star forming clouds in galaxies, and that the properties of the dense clouds are relatively universal (Wu et al. 2005).

The emission lines from the dense gas tracers are typically an order of magnitude weaker than CO, although the ratio varies dramatically between galaxies (Gao & Solomon 2004). A few galaxies have been detected in the dense gas tracers at high redshift, predominantly strongly gravitationally lensed systems (Riechers et al. 2011a,b; Wagg et al. 2005, Carilli et al. 2005; Solomon et al. 2003). The high redshift galaxies generally follow the low redshift correlations. Interestingly, in some cases even the high order transitions are excited, indicating either extremely dense gas, or a contribution to the excitation by the AGN (Riechers et al. 2011a,b; Wagg et al. 2005).

4.3. Topics on quasar hosts

4.3.1. Dust and molecular gas in the most distant galaxies

Detection of molecular line emission at the very highest redshifts ($z > 6$) has thus far been limited to quasar host galaxies. These galaxies generally follow the trends discussed above for SMGs and lower redshift quasar hosts in terms of their warm dust and molecular gas properties, and in particular, the 1/3 fraction of submm detections of quasar host galaxies at $S_{250GHz} \geq 2$mJy remains constant to the highest redshifts, implying HyLIRG host galaxies.

Figure 8 shows the SED of the most distant SDSS quasar J1148+5258 from UV to radio wavelengths. This SED is typical of the submm detected high z quasars (Wang et al. 2009, 2010; Leipski et al. 2010). From the UV through mid-IR ($\sim 30\mu$m rest frame), the SED is consistent with that of lower redshift SDSS quasars, including a hot dust (1000K) seen in the mid-IR, heated by the AGN. However, the submm detected sources show a substantial excess over the lower z SDSS quasar SED. This excess is well fit by a warm dust component ($\sim$ 50K). Extrapolating this component to the radio also shows that most of the sources follow the radio-FIR correlation for star forming galaxies. These results argue that the warm dust component is heated by star formation in the host galaxy. The star formation rates are $\sim 10^3$ M$_\odot$ year^{-1}, implying a major starburst

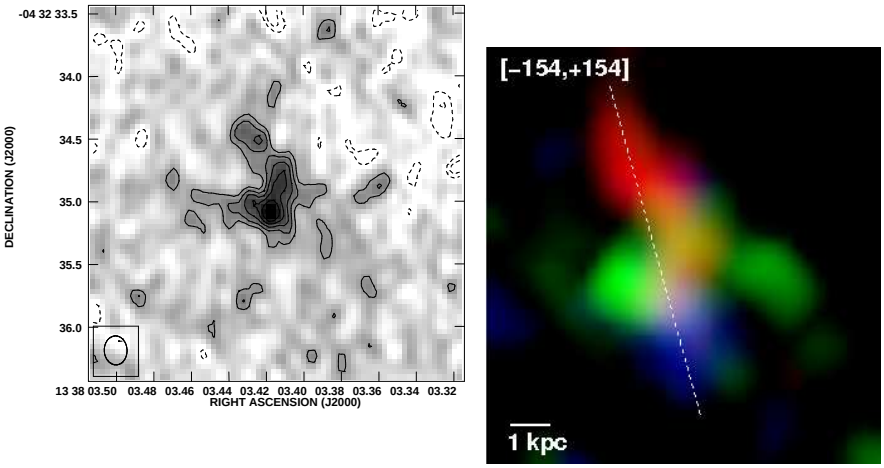

Fig. 7.— The CO emission from the $z = 4.4$ quasar host galaxy BRI1335-0417 (from Riechers et al. 2008). Left is the velocity integrated intensity and right the mean CO velocity.

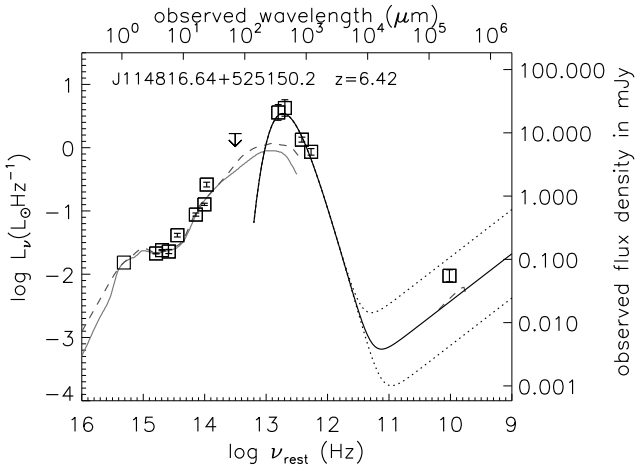

Fig. 8.— The UV through radio SED of the $z = 6.42$ quasar J1148+5258 (from Wang et al. 2008). The curves in the UV through mid-IR are local quasar templates from Elvis et al. (1994) and Richards et al. (2006). The curves in the Far-IR through radio are for a 50K dust model that obeys the radio-FIR correlation for star forming galaxies.

coeval with the AGN in the host galaxy.

CO has been detected in every $z \sim 6$ quasar host galaxy that was selected via a previous submm detection of the dust. To date, 11 quasar host galaxies have been detected in CO emission between $z = 5.7$ and 6.4 (Wang et al. 2010), with gas masses $\geq 10^{10}$ $M_\odot$.

The detection of large dust masses within 1Gyr of the Big Bang immediately raises an interesting question: how does so much dust form so early? One standard dust formation mechanism in the ISM involves coagulation in the cool winds from low mass stars, which, naively would take too long. The large dust masses have led to a number of theoretical studies of early dust formation, with models involving: dust formation associated with massive star formation in eg. supernova remnants (Dwek et al. 2007; Venkatesen et al 2006), dust formation in outflows from the broad line regions of quasars (Elitzur in prep; Elvis et al. 2002), and dust formation in the gas phase ISM (Draine 2003). Michalowski et al. (2010) consider this problem in detail, and show that AGB stars are insufficient, and even SNe require a very top-heavy IMF and unrealistic dust yields.

Recent observations of the UV-extinction curves in a few $z \sim 6$ quasars and GRBs suggest a different dust composition at $z > 6$ relative to the Milky Way or the SMC, as well as relative to quasars at $z < 4$. The extinction can be modeled by larger silicate and amorphous carbon grains (vs. eg. graphite), as might be expected from dust formed in supernova remnants (Stratta et al. 2007; Perley et al. 2010). The formation of dust in the early Universe remains an interesting open question.

4.3.2. Fine structure lines: [CII] 158μm

At high redshift the FIR atomic fine structure lines are observed in the submm band, and hence can be studied with existing ground-based telescopes. In particular, substantial progress has been in the study of [CII] in distant galaxies.

We have started a systematic search for [CII] emission from $z > 4$ quasars quasar host galaxies (Maiolino et al. 2005; Wagg et al. 2010). At the highest redshifts, we now have three detections of the [CII] line from $z > 6.2$ quasar host galaxies (Bertoldi et al. in prep).

Figure 9 shows the [CII] images of the $z = 6.42$ quasar J1148+5258, as well as the mm continuum and VLA CO 3-2 images, at 0.25" resolution from the PdBI (Walter et al. 2009). The [CII] emission is extended over about 1.5 kpc, while the CO is even more extended. If [CII] traces star formation, the implied star formation rate per unit area $\sim 10^3$ $M_\odot$ year^{-1} kpc^{-2}. This value corresponds to the predicted upper limit for a 'maximal starburst disk' by Thompson et al. (2005), ie. a self-gravitating gas disk that is supported by radiation pressure on dust grains. Such a high star formation rate areal density has been seen on pc-scales in Galactic GMCs, as well as on 100 pc scales in the nuclei of nearby ULIRGs. For J1148+5251 the scale for the disk is yet another order of magnitude larger.

One potential difficulty with using the [CII] line as a star formation diagnostic is the very broad range in the ratio of [CII] to Far-IR luminosity, in particular for galaxies with $L_{FIR} > 10^{11}$ $L_{\odot}$. Stacey et al. (2011) present an analysis of this ratio versus L_{FIR} for low and high redshift galaxies. At high luminosity, the distribution is essentially a scatter plot, with the ratio ranging by 3 orders of magnitude, although there appears to be less scatter if AGN are removed. Figure 10 shows this ratio versus dust temperature. Malhotra et al. (2001) consider temperature to be the more fundamental quantity, due to inefficiency of photoelectric heating of charged dust grains in high radiation environments. Figure 10 shows a possible correlation of the [CII] to L_{FIR} ratio with dust temperature, but again, the scatter is very large. Papadopoulos et al. (2010) also point out that dust opaticy might play a role in decrease the [CII] luminousity from extreme starburst galaxies.

4.3.3. The Black Hole – Bulge mass relation within 1 Gyr of the Big Bang

There is a well studied correlation between the masses of black holes at the centers of galaxies, and the velocity dispersion of the host galaxies. This M_{BH} - σ_V relation implies a roughly linear correlation between black hole and spheroidal galaxy mass, with a proportionality constant of: $M_{BH} = 0.002 M_{bulge}$. This correlation has been used to argue for a 'causal connection between the formation of supermassive black holes and their host spheroidal galaxies' (Gebhardt et al. 2000; Kormendy & Bender 2011; Häring & Rix 2004; Gultekin et al. 2009). While AGN feedback via winds or jets has been invoked to explain the effect, the details remain obscure.

High resolution imaging of gas dynamics allows for study of the evolution of the black hole – bulge mass relation to high redshift redshift. Imaging of a few $z \geq 4$ quasars shows a systematic departure from the low z relationship (eg. Walter et al. 2004; Riechers et al. 2008). Figure 11 shows a compilation by Wang et al. (2010). They find that, assuming random inclination angles for the molecular gas, the $z \sim 6$ quasars are, on average, a factor 15 away from the black hole – bulge mass relation, in the sense of over-massive black holes. Alternatively, all of the $z \sim 6$ quasars could be close to face-on, with inclination angles relative to the sky plane all $< 20^{o}$. High resolution imaging of the CO emission from these systems is required to address the interesting possibility that the black holes form before the host spheroids.

4.4. Massive galaxy formation at high redshift

Overall, the observations of the molecular gas and dust in extreme starburst galaxies at high redshift (SMGs, AGN hosts) indicate a major star formation episode during the formation of massive galaxies in group or cluster environments.

A key question is: what drives the prolific star formation? Tacconi et al. (2006; 2008) argue, based on imaging of higher-order CO emission from a sample of $z \sim 2$ SMGs, that SMGs

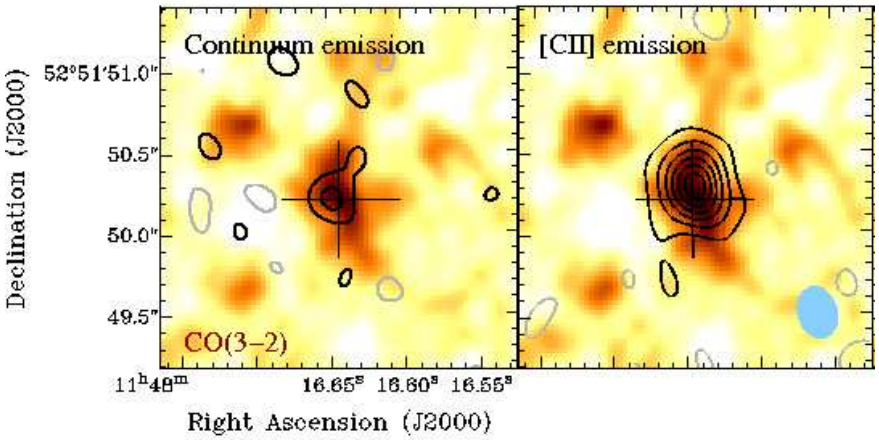

Fig. 9.— The images of the $z = 6.42$ quasar J1148+5251. Images from the PdBI show the dust and [CII] emission (contours, left and right, respectively) at 0.25" resolution, plus the VLA CO 3-2 in color (from Walter et al. 2009; 2004).

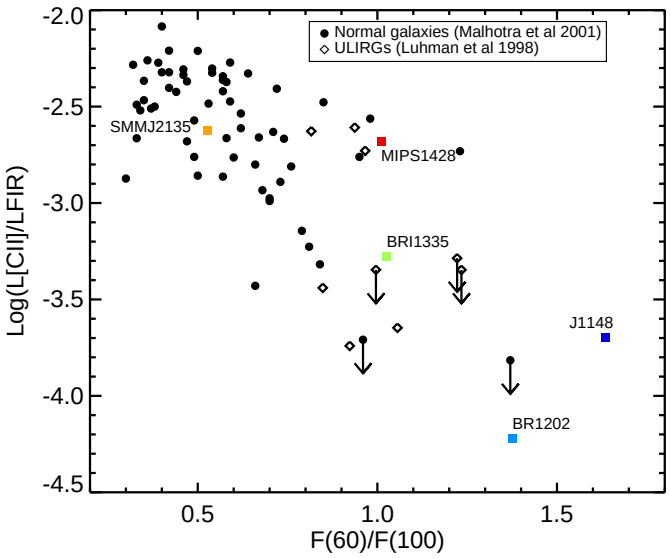

Fig. 10.— The [CII]/L_{FIR} ratio versus dust temperature for low and high redshift galaxies (Wagg et al. in prep.).

are predominantly nuclear starbursts, with median sizes < 0.5" ($<$ 4kpc), 'representing extreme, short-lived, maximum star forming events in highly dissipative mergers of gas rich galaxies.' This conclusion is supported by VLBI imaging of the 1.4 GHz emission from star forming regions in two SMGs (Momjian et al. 2005; 2010).

However, recent EVLA imaging of the lower order CO emission in SMGs (Ivison et al. 2011; Carilli et al. 2010; Riechers et al. 2011c), suggests that the lower-excitation molecular gas reservoirs can be significantly more extended. Riechers et al. (2011c) suggest a sequence in which the SMG phase is an early stage of a major gas rich merger, with the quasar phase arising later in the evolution (Sanders et al. 1988).

5. Secular galaxy formation during the epoch of galaxy assembly

5.1. sBzK and other typical star forming galaxies at $z \sim 1$ to 3

Optical through near-IR color selection techniques have become remarkably efficient at finding both star forming and passive galaxies during the peak epoch of galaxy assembly ($z \sim 1$ to 3). These include (rest frame) UV-selected samples (BX/BM; Steidel et al. 2004) and near-IR selected samples (sBzK; Daddi et al. 2005). Grazian et al. (2003) analyze the substantial overlap between the populations. The critical aspect for these samples is that they are not rare, pathological galaxies, such as luminous quasar hosts or the hyper-starburst submm galaxies. These galaxy samples are generally representative of the broad distribution of star forming galaxies at these epochs (Section 1), with areal densities of a few arcmin^{-2}, or volume densities $\geq 10^4$ Mpc^{-3}.

HST imaging of these galaxies show clumpy but predominantly disk-like galaxies with sizes of order 10 kpc (Figure 12; Daddi et al. 2010a), with stellar masses $\geq 10^{10}$ M$_\odot$. Imaging of the Hα and CO emission, reveals turbulent, but systematically rotating gas disks, and giant star forming clumps up to 1kpc in size (Genzel et al. 2008, 2011; Förster-Schreiber et al. 2011; Tacconi et al. 2010).

5.2. COSMOS radio stacking: dawn of downsizing

Pannella et al. (2010) have selected a sample of 30,000 sBzK galaxies from the COSMOS survey to determine the mean dust-unbiased star formation rates using stacking of 1.4 GHz observations. The number of sources, and the sensitivity of the radio observations, allow for substantial binning of the galaxies as a function of stellar mass, star formation rate, color, and blue magnitude. There is no correlation between median star formation rate and blue magnitude. This lack of correlation of SFR with blue magnitude occurs because there is a strong correlation of star formation rate with B-z color, ie. the extinction increases with star formation rate. There is also a positive correlation of star formation rate with stellar mass.

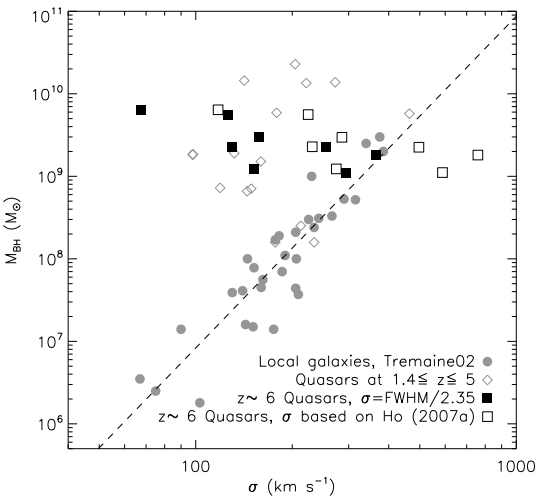

Fig. 11.— The relationship between the black hole mass and the host spheroidal galaxy velocity dispersion for low and high redshift quasars (from Wang et al. 2010a). For the high z sources the velocity dispersion is estimated from the CO line imaging.

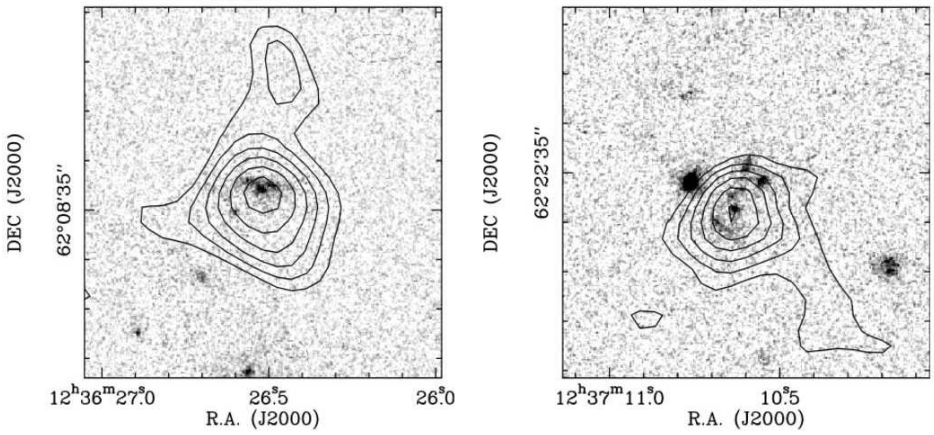

Fig. 12.— The CO emission from two $z \sim 1.5$ sBzK galaxies, with two CO velocity intervals shown as contours, and the greyscale is the HST i-band image (from Daddi et al 2010a).

Combining these data, Figure 13 shows the specific star formation rate (SFR/M_{stars}) versus stellar mass for the COSMOS sBzK sample. For comparison, the relation at $z = 0.3$ from Zheng et al. (2007) is also shown. A line shows the inverse Hubble time at $z = 1.8$. Galaxies above this line have SSFR that are sufficient to form the observed stars in the galaxy over their Hubble time. Galaxies below this line required a substantial increase in SFR rate in the past to form the stars that are seen. Lastly, the open points showing the SSFR based on dust-uncorrect star formation rates from the UV measurements.

From Figure 13, the SSFR increases with redshift, even between $z = 1.5$ and 2.1. The high redshift galaxies are all above the 'red and dead' line indicated by the inverse Hubble time. Pannella et al. find that the substantial negative slope with stellar mass seen at $z = 0.3$ (ie. the decrease in SSFR with increasing stellar mass) becomes essentially flat at $z \geq 1.5$. Hence, $z \sim 2$ corresponds to an epoch when even fairly massive but common galaxies are actively forming stars. Lastly, it is clear that the dust extinction increases with increasing star formation rate. Interestingly, the standard factor 5 UV extinction correction for LBGs occurs at a stellar mass of $\sim 2 \times 10^{10}$ $M_{\odot}$, which is typical of LBG samples (Shapley et al. 2003).

5.3. Molecular gas: gas-dominated galaxies

Perhaps the most interesting result from the study of the sBzK and BX/BM galaxy samples comes from the searches for molecular gas. These samples show a remarkably high detection rate ($> 50\%$), in CO emission (Daddi et al. 2010a; Tacconi et al. 2010). The line strengths are comparable to those seen in SMGs and quasar hosts, but the star formation rates are an order of magnitude smaller. Figure 12 shows some examples. High resolution imaging shows that the CO is extended on the same scale as the optical disks, ($\sim$ 10kpc), with large condensations of size $\sim$ 1kpc, and masses $> 10^9$ $M_{\odot}$ (Tacconi et al. 2010; Aravena et al. 2010; Daddi etal. 2009a).

Some of these galaxies have been observed in the CO 1-0 transition with the VLA, as well as higher order transitions with the PdBI (Figure 14; Dannerbauer et al. 2009; Aravena et al. 2010). The excitation up to CO 3-2 appears to be sub-thermal, and substantially lower than is seen in either quasar hosts and SMGs (Figure 6). The excitation up to CO 3-2 is comparable to the Milky Way disk. Likewise, Figure 15 shows that the ratio of CO luminosity to FIR luminosity in these galaxies is similar to the Milky Way, and not to the SMG population, or compact nuclear starbursts.

Daddi et al. (2010a) have done a detailed analysis of the possible CO luminosity to H_2 mass conversion for the sBzK sample. They employ dynamical models of forming disk galaxies including dark matter, as well as extensive observations of the stellar content and the CO dynamics. They conclude that the CO conversion factor is likely similar to the Milky Way value, rather than the nuclear starburst value employed for SMGs and quasar hosts. This conclusion is consistent with the Milky Way-like excitation and $L'CO/L_{FIR}$ ratio, and the large scale for the CO disks. Tacconi

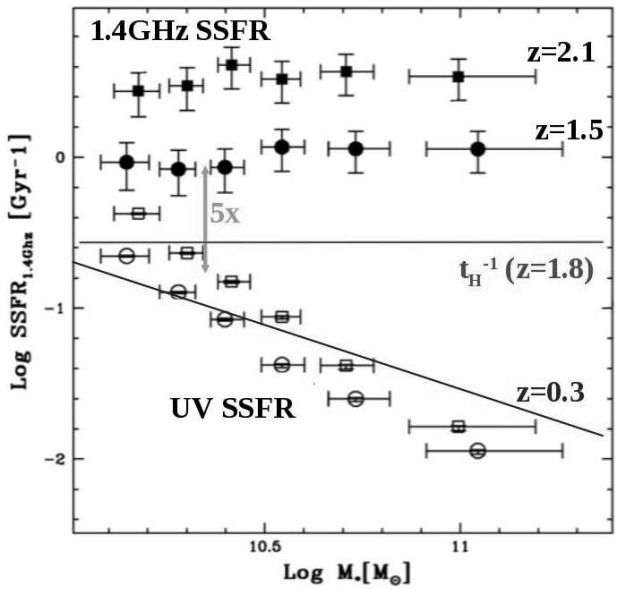

Fig. 13.— The specific star formation rate for $z \sim 2$ COSMOS sBzK galaxies (Pannella et al. 2009). Black filled symbols are SFR results from stacking of 1.4 GHz emission. Open symbols are the UV derived SFR without an extinction correction. A line indicates the SSFR vs. stellar mass for $z \sim 0.3$ galaxies in the Zheng et al. (2007) sample.

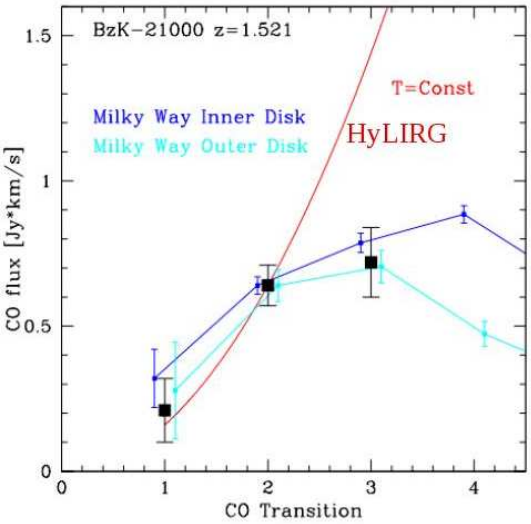

Fig. 14.— The CO ladder for sBzK galaxies (CO flux versus rotational quantum number for the upper state. The redline indicates constant brightness temperature (flux $\propto \nu^2$), typical for SMGs and AGN hosts in this J range (Dannerbauer et al. 2009; Aravena et al. 2010).

et al. (2010) reach a similar conclusion on α for the BX/BM samples.

The implied H_2 masses are then of order 10^{11} $M_\odot$. The gas masses are comparable to, or larger than stellar masses in the sBzK and BX/BM samples (Daddi et al. 2010a; Tacconi et al. 2010). This is very different with respect to low redshift disk galaxies, where the baryon content is dominated by stars (Figure 16). Hence, the peak epoch of cosmic star formation also corresponds to an an epoch when the dominant baryon component in star forming galaxies is gas, not stars.

5.4. Normal galaxy formation in the gas rich-era

The implied gas consumption timescales for the sBzK and BX/BM galaxies is $\sim$ few$\times 10^8$ years. This is an order of magnitude longer than the gas consumption timescale for the hyperstarbursts in SMGs and quasar host galaxies. Genzel et al. (2010) consider this point in detail, and conclude that the most likely explanation relates to different global dynamical effects in disks versus compact starbusts. They also emphasize that the gas consumption timescales are much shorter than the Hubble time in either case, and hence star formation must be a balance between gas accretion and feedback (see also Bauermeister et al. 2010).

Theoretical and numerical studies have recently suggested that the dominant mode of star formation in the Universe, again peaking around $z \sim 1$ to 3, is not related to major gas rich merger events, but is driven by the slower process of 'cold mode accretion' (Dekel et al. 2009; Keres et al. 2009). In the CMA model, gas flows into galaxies from the IGM along cool, dense filaments. The flow never shock-heats due to the rapid cooling time, but continuously streams onto the galaxy at close to the free-fall time. This gas forms a thick, turbulent, rotating disk which efficiently forms stars across the disk, punctuated by giant clouds of enhanced star formation on scales $\sim$ few kpc. Genzel et al. (2008; 2011) show that the process is consistent with marginally Toomre-unstable gaseous disks. These star forming regions then migrate to the galaxy center via dynamical friction and viscosity, forming compact stellar bulges (Genzel et al. 2008; Bournaud et al. 2009; Elmegreen et al. 2009). The process is regulated by feedback, both within the giant star forming clouds themselves, and possibly from an active nucleus (Dave et al. 2011; Genzel et al. 2010).

The CMA process leads to relatively steady and active ($\sim$ 100 $M_\odot$ yr^{-1}) star formation in galaxies over timescales approaching 1 Gyr. The process slows down dramatically as gas supply decreases, and the halo mass increases, generating a virial shock in the accreting gas. Subsequent dry mergers at lower redshift then lead to continued total mass build up, and morphological evolution, but little subsequent star formation.

The Hα and CO dynamical analyses of these samples are generally consistent with the morphologies expected from CMA, including turbulent but systematically rotating, gas disks, and giant star forming clumps. Shapiro et al. (2008) show that such a study of disk kinemetry enables an 'empirical differentiation between merging and non-merging systems'. Of course, this remains just a consistency check, and not direct observation of CMA.

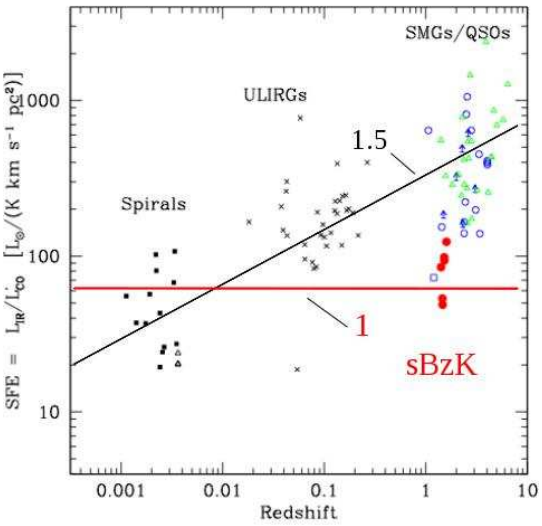

Fig. 15.— The ratio of FIR to CO luminosity for sBzK galaxies (red), and other galaxy samples (from Daddi et al. 2010a). The lines indicate powerlaw relationships of different indices.

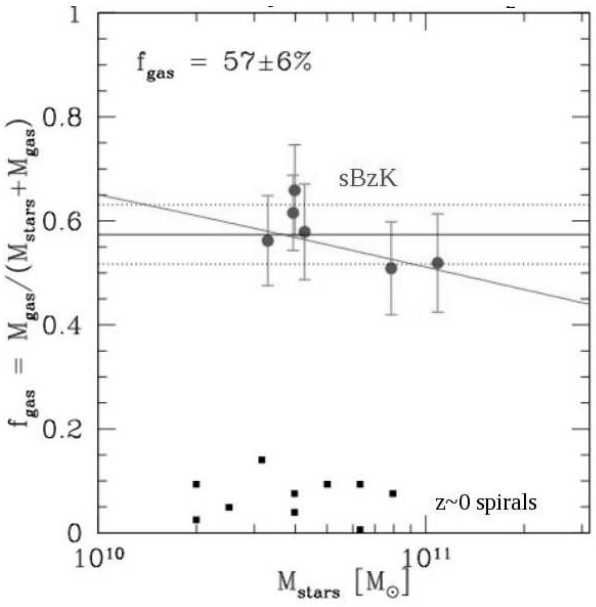

Fig. 16.— The molecular gas baryon fraction for sBzK galaxies at $z \sim 1.5$ (circles), and low redshift spirals (squares; from Daddi et al. 2010a)).

Interestingly, observations of even more luminous star forming galaxies at even high redshift ($z > 4$) suggest that CMA may scale up to SMG lumnosities at the highest redshifts (Carilli et al. 2010).

6. Dense gas history of the Universe

While admittedly compressing much information, the star formation history of the Universe has been a dominant tool in the study of galaxy formation over the last decade (Figure 1). However, the relationship between star formation and the molecular gas content of galaxies (Figure 2), implies that the SFHU should be reflected in the evolution of molecular gas.

Section 5.3 discusses how the average molecular gas content of star forming galaxies rises substantially with redshift. This is quantified in Figure 17, which shows the mean molecular gas baryon fraction ($\equiv M_{gas}/[M_{gas} + M_{stars}]$), for star forming galaxies with $M_{stars} > 10^{10}$ $M_\odot$ (adapted from Daddi et al. 2010b; Geach et al. 2011; Bauermeister et al. 2010). Admittedly there are many selection effects and assumptions that enter this calculation, but the current data support the idea of a substantial increase in the molecular gas content of galaxies at the peak epoch of cosmic star formation.

The next level of abstraction is to sum the gas mass to obtain the evolution of the cosmic density of molecular gas. Figure 18 shows an initial, very gross attempt at such a calculation, based on the 115 CO detections at $z > 1$ to date. The gas mass calculation entails a simple scaling from stellar mass densities from Grazian et al. (2007) using the mean gas baryon fraction for the different samples (Daddi et al. 2009b; Tacconi et al. 2010; Riechers et al. 2010b). We include the $z = 0$ value from Keres et al. (2003). This figure includes two basic models: one boot-strapped from the SFHU plot assuming a constant timescale for gas conversion to stars in galaxies (Bigiel et al. 2011; Leroy et al. 2008; Bauermeister et al. 2010). The second is based on the work of Obreschkow and Rawlings (2009), who predict the molecular gas content of galaxies based on the Millenium simulations.

We emphasize this plot remains highly speculative due to the many assumptions involved, in particular, the conversion factor of CO luminosity to molecular gas mass, the open question of the evolution of the star formation law, and very limited samples.

7. ALMA and EVLA

The last decade has seen the opening of the high z Universe to radio observations of the dust, gas, and star formation in the first galaxies. These results emphasize the critical need for pan-chromatic studies of galaxy formation to reveal all the key elements of the complext process. Fortunately, the immediate promise for a dramatic improvement in these studies is being real-

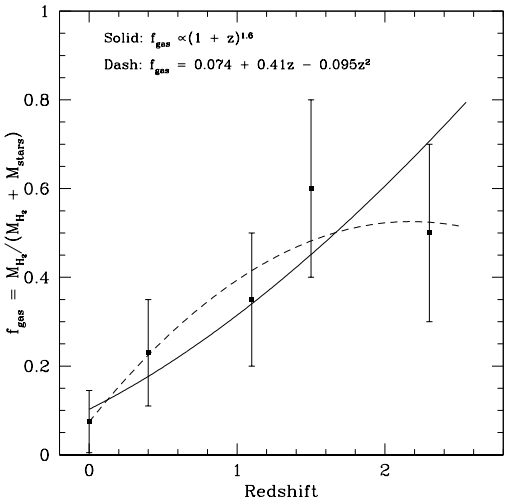

Fig. 17.— The molecular gas baryon fraction for star forming galaxies with $M_{stars} \geq 10^{10}$ $M_{\odot}$ (adapted and revised from Daddi et al. 2010a; Geach et al. 2011; Bauermeister et al. 2010).

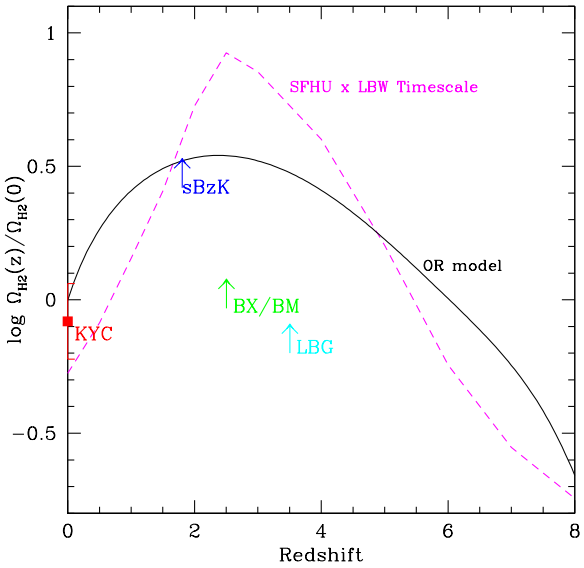

Fig. 18.— Gross estimates of the cosmic density (comoving) of molecular gas versus redshift based on the samples of star forming galaxies observed at $z > 1$. These include the near-IR selected sBzK galaxies (Daddi et al. 2010a), optically selected (BX/BM) galaxies (Tacconi et al. 2010; Genzel et al. 2010), and LBGs (Riechers et al. 2010b). Also plotted are two basic models: one boot-strapped from the SFHU plot assuming a simple timescale for gas conversion to stars in galaxies (Leroy et al. 2008). The second is based on the work of Obreschkow and Rawlings (2009) and the Millenium simulations. The zero redshift point is from the CO survey of Keres et al. (2003).

ized with the science commissioning of the Expanded Very Large Array and the Atacama Large Millimeter Array.

The EVLA is a complete reinvention of the VLA, building on existing infrastructure (telescopes, rail track), but completely replacing the entire (1970's) electronic systems, from receivers through LO/IF to the correlator, to establish an essentially completely new telescope for the coming decade (Perley et al. 2011). The EVLA has complete frequency coverage from 1 GHz to 50GHz, and the bandwidth has increased by a factor 80, to 8GHz with thousands of spectral channels, greatly improving capabilities for spectral line searches and studies. The continuum sensitivity has increased by up to an order of magnitude. The array still provides compact configurations to image larger structures, and extended configurations that provide resolutions down to 40mas at 40GHz.

The EVLA construction project is close to completion, and the full array is operating at ≥ 18 GHz with up to 2 GHz of bandwidth. Early science observations have been proceeding since March 2010, and indeed, some of the results discussed above are based on these observations.

The ALMA telescope will consist of 54 12m antennas for sensitive observations, plus 12 7m antennas for wide field imaging (Wootten & Thompson 2009), located at one of the best submm observing sites in the world, at 5000m elevation in Chile. The array will work from 80GHz to 750 GHz, initially in four bands, with an instantaneous bandwidth of 8GHz. The array configurations can be adjusted for wide field imaging as well as high resolution imaging to 20mas resolution at 350 GHz. Figure 4 shows the sensitivity of ALMA compared to existing (sub)mm arrays. The 3 orders of magnitude improvement in sensitivity in the submm is particularly dramatic.

The ALMA is also well into construction, with about half the antennas either operating at the high site, or under construction at the observational support facility. Demostration science observations have already shown the power of even a limited set of ALMA antennas to perform ground-breaking observations of the dust and gas in galaxies, and early science observations will start at the end of 2011.

Taken together, ALMA and the EVLA represent an order of magnitude, or more, improvement in observational capabilities from 1 GHz up to 1 THz. Such a jump in capabilities is essentially unprecedented in ground-based astronomy. Following are a few examples of the potential of these instruments.

Figure 19 shows the sensitivity of ALMA, and other telescopes, to the [CII] line emission versus redshift. Included are the expected signals of star forming galaxies of different luminosity. ALMA will detect the [CII] line from typical LBGs well into cosmic reionization. Indeed, the 8GHz bandwidth and sensitivity present the interesting potential for determining the redshifts for these first galaxies. Determining optical spectroscopic redshifts is particularly hard as the Lyα line shifts into the near-IR, and the presence of a partially neutral IGM can attenuate the Lyα emission as well.

Figure 20 shows what an 8GHz spectrum of a luminous starburst, like J1148+5258 at $z = 6.42$,

might look like with ALMA. Numerous interesting transitions of important diagnostic molecules will be detected, including dense gas tracers, isotopes, and isomers. ALMA opens up full astrochemical studies of the first galaxies.

The EVLA has a 25% fractional bandwidth at 30 GHz. Hence, every observation with the EVLA at high frequency will include a blind search for molecular line emitting galaxies at high redshift. For instance, an EVLA observation at 19 to 27 GHz covers CO 1-0 at $z = 3.2$ to 5.0 instantaneously, thereby obviating the need for optical spectroscopic redshifts. Figure 21 shows a recent example from EVLA early science of this potential. Three molecule rich galaxies have been observed in a single pointing and 256MHz bandpass with the EVLA. Essentially every long observation of the EVLA over 20GHz will detect molecular line emission from distant galaxies, whether intended or not.

CC thanks the Astronomische Gesellschaft organizers for their hospitality. We thank A. Weiss and R. Bouwens for figures.

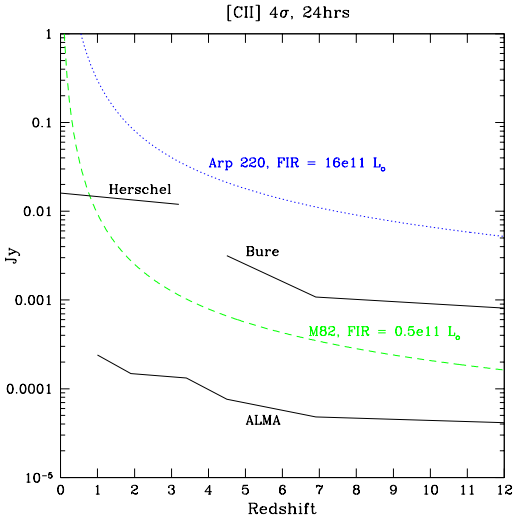

Fig. 19.— The expected [CII] line peak flux density versus redshift for active and dwarf star forming galaxies, plus the sensitivity of ALMA and other instruments. Note that there are gaps in the frequency coverage due the atmostphere and availability of receivers that are not depicted.

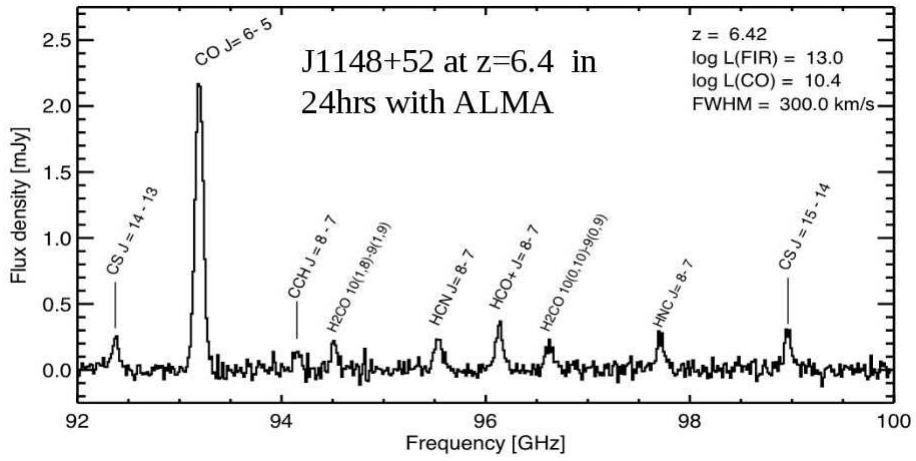

Fig. 20.— A simulated spectrum of the HyLIRG J1148+5258 at $z = 6.42$ with 8GHz using ALMA in 24 hours.

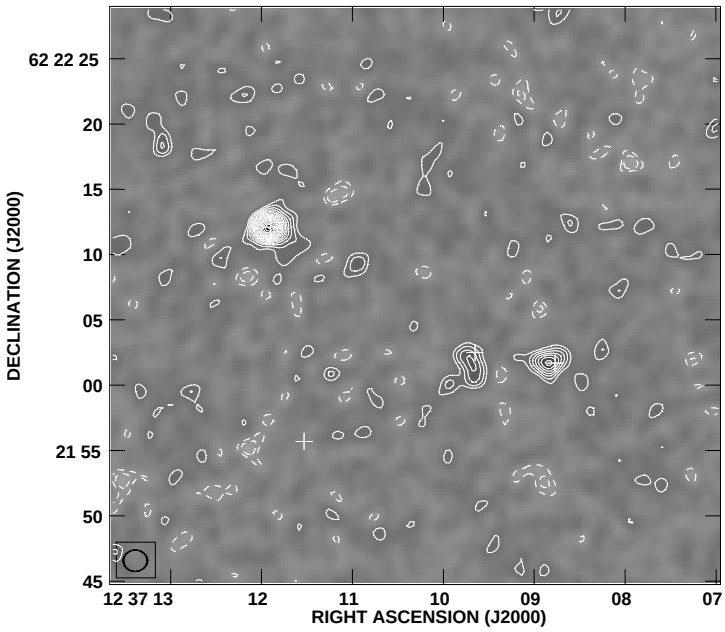

Fig. 21.— The GN20 field seen with the EVLA with a 256 MHz bandwidth at 45 GHz. Three galaxies are detected in CO 2-1 emission at $z = 4.0$ (from Carilli et al. 2011).

Amblard, A. et al. 2011, Nature, 470, 510

Andreon, S. & Huertas-Company, M. 2011, A& A, 526, 11

Aravena, M., Bertoldi, F., Carilli, C. et al. 2010, ApJL, 708, L36

Baker, A. et al. 2004, ApJ, 613, L113

Bauermeister, A. et al. 2010, 717, 323

Blain, A. et al. 2002, PhR 369 111

Bennett, C. et al. 1994, ApJ, 434, 587

Bertoldi, F. et al. 2010 COSMOS mm

Bigiel, F. et al. 2011, 730, L13

Bournaud, F. et al. 2009, ApJ, 707, L1

Bourne, N. et al. 2011, MNRAS, 410, 1155

Bouwens, R. et al. 2010, ApJ, in press, arXiv 1006.4360

Calzetti, D. et al. 1994, ApJ, 429, 582

Carilli, C.L. et al. 2008, ApJ, 689, 883

Carilli C.L. et al. 2010, 714, 1407

Carilli C.L. et al. 2002, AJ, 123, 1838

Carilli C.L. 2011, ApJ, 730, L30

Carilli C.L. et al. 2011, ApJL, in press

Carilli, C.L. et al. 2005, ApJ, 618, 586

Chapman, S., Blain, A., Ivison, R., Smail, I. 2003 Nature 422 695

Chapman, S., Blain, A., Ibata, R. et al. 2009, ApJ, 691, 560

Collins, D., Stott, J.P., Hilton, M. et al. 2009, Nature, 458, 603

Coppin, K, et al. 2010, MNRAS, 407, L103

Coppin, K, et al. 2010, ApJ, 665, 936

Cormier, D. et al. 2010, A& A, 518, L57

Cowie, L. et al. 1997, 481, L9

Daddi, E. et al. 2004, ApJ, 617, 746

Daddi, E., Dickinson, M., Chary, R. et al 2005, ApJ 631 L13

Daddi, E., Dannerbauer, H., Stern, D. et al. 2009a, ApJ, 694, 1517

Daddi, E., Dannerbauer, H., Krips, M. et al. 2009b, ApJ, 695, L176

Daddi, E. et al. 2010a, ApJ, 713, 686

Daddi, E. et al. 2010b, ApJ, 714, L118

Dannerbauer, H., Walter, F., Morrison, G. 2008, ApJ, 673, L127

Dave, R. et al. 2011, MNRAS, in press ArXiv1103.3528

Dekel, A. et al. 2009, ApJ, 703, 785

Downes & Solomon 1998 ApJ, 507, 615

Doherty, M., Tanaka, M., de Breuck, C. et al. 2009, A& A, 509, 83

Draine, B. 2003, ARAA 41 , 241

Dwek, E. et al. 2007, ApJ 662 , 927

Elvis, M. et al. 1994, ApJS, 95, 1

Elvis, M. et al. 2002, ApJ 567 , L107

Elmegreen, B. et al. 2009, 692, 12

Fan, X., Carilli, C. Keating, B. 2006, ARAA, 44, 415

Förster-Schreiber, N. et al. 2011, ApJ, in press, arXiv1104.0248

Geach, J. et al. 2011, ApJ, 730, L19

Gao, Y. & Solomon, P. 2004, ApJ 606 , 271

Gebhardt, K. et al. 2000, ApJ, 543, L5

Genzel, R. & Cesarsky, C. 2000, ARAA, 38, 761

Genzel, R. et al. 2011, ApJ, in press ArXiv 1011.5360

Genzel, R. et al. 2010, MNRAS, 407, 2091

Genzel, R. et al. 2008, ApJ, 687, 59

Grazian, A. et al. 2007, A& A, 465, 393

Gultekin, K. et al. 2009, 706, 404

Hainline, :. et al. 2006, ApJ, 650, 614

Häring, N. & Rix, W. 2004, ApJ 604 , L89

Harris, A. et al. 2010, ApJ, 723, 1139

Ivison, R. et al. 2011, MNRAS, 412, 1913

Kennicutt, R. 1998, ARAA, 36, 189

Keres, D., Yun, M.S., Young, J. 2003, ApJ, 582, 659

Keres, D. et al. 2009, MNRAS, 395, 160

Kormendy, J. & Bender, R. 2011, Nature, 469, 377

Krumholz et al. 2009, ApJ, 699, 850

Kurk, J., Cimatti, A., Zamorani, G. et al. 2009, A& A, 504, 331

Leroy, A. et al. 2008, 136, 2782

Leipski, C. et al. 2010, A& A, 518, L34

Madau, P. et al. 1996, MNRAS, 283, 1388

Maiolino, R. et al. 2005, A& A 40 , L51

Malhotra, S. et al. 2001, ApJ, 561, 766

Marchesini, D. et al. 2009, ApJ, 701, 1765

Magnelli, B. et al. 2011, A& A, 528, 35

Michalowski, M. et al. 2010, A& A, 522, 15

Michalowski, M. et al. 2010, A& A, 515, 67

Miley, G. & de Breuck, C. 2008, A& ARv, 15, 67

Momjian, E., Carilli, C. & Petric, A. 2005, AJ, 129, 1809

Momjian, E. et al. 2010, AJ, 139, 1622

Moresco, M. et al. 2010, A& A, 524, 67

Murphy, E. et al. 2011, ApJ, in press arXiv1102.3920

Narayanan, D. et al. 2011, ApJ, in press arXiv 1104.4118

Obreschkow, D. & Rawlings, S. 2009, ApJ, 696, L129

Pannella, M. et al. 2009, ApJ, 698, 116

Papadopoulos, P. et al. 2002, ApJ, 564, L9

Papadopoulos, P. et al. 2010, ApJ, 711, 757

Perley, R. et al. 2011, ApJL, in press

Perley, D. et al. ApJ in press (2010)

Renzini, A. 2006, ARAA, 44, 141

Richards, G.T. et al. 2006, ApJS, 166, 470

Riechers, D. et al. 2008, ApJ, 686, L9

Riechers, D. et al. 2010a, ApJL, 720, L131

Riechers, D. et al. 2010b, ApJ, 724, L153

Riechers, D. et al. 2011a, ApJ, 726, 50

Riechers, D. et al. 2011b, ApJ, 725, 1032

Riechers, D. et al. 2011b, ApJ, in press arXiv1104.4348

Sanders, D. et al. 1988, ApJ, ApJ 325, 74

Schinnerer, E. et al. 2008, ApJ, 689, L5

Scott, K. et al. 2011, ApJ, in press, arXiv1104.4115

Shapiro, K. et al. 2008, ApJ, 682, 231

Shapley, A. et al. 2003, ApJ, 651, 688

Spitzer, L. 1998, *Physical Processes in the Interstellar Medium,* (Wiley)

Solomon, P. & Vanden Bout, P. 2005, ARAA, 43, 677

Solomon, P. et al. 2003, Nature, 426, 636

Stacey, G. et al. 2010, ApJ, 724, 957

Stratta, G. et al. 2007, ApJ 661 , L9

Steidel, C. et al. 2004, ApJ, 604, 534

Tacconi, L., Neri, R., Chapman, S. et al. 2006, ApJ, 640, 228

Tacconi, L., Genzel, R., Smail, I., et al. 2008, ApJ, 680, 246

Tacconi, L. et al. 2010, Nature, 464, 781

Thompson, T. et al. 2005, ApJ 630 , 167

Venkatesan, A. et al. ApJ 640 , 31 (2006)

Wagg, J. et al. 2010, A& A, 519, L1

Wagg, J. et al. 2005, ApJ, 634, L13

Walter, F. et al. 2009, Nature 457 , 699

Walter, F et al. 2004, ApJ 615 , L17

Walter, F. et al. 2003, Nature 424 , 406

Wang, R. et al. ApJ 714 , 699 (2010b)

Wang, R. et al. ApJ 687 , 848 (2008)

Weiss, A. et al. 2007, ASPC, 375, 25

Wootten, A. & Thompson, A. 2009, IEEEP, 97, 1463

Wu, J. et al. 2005, ApJ, 635, L173

Yun, M.S. et al. 2001, ApJ 554 , 803

Zheng, X. et al. 2007, ApJ, 661, L41